Journal of the Korean Magnetic Resonance Society **2005**, *9*, 74 - 92

The High Resolution NMR Solution Structure of Monocyte Chemoattractant Protein-3

DoYoon Kwon[1], DuckYeon Lee[1], Brian D. Sykes[2] and Key-Sun Kim[1*]

[1]Biomedical Research Center, Korea Institute of Science & Technology, Seoul, 130-650, and [2]Protein Engineering Network of Centres of Excellence (PENCE) & Dept. of Biochemistry, Univ. of Alberta, Edmonton, Alberta, Canada T6G 2S2

Received July 5, 2005

Abstract : The high resolution solution structure of MCP-3 was determined using multinuclear, multidimensional NMR spectroscopy with an expressed and ^{13}C- and ^{15}N-labeled protein. The MCP-3 has a typical chemokine fold including 3 anti-parallel β-sheets, and a C-terminal helix, but it exists as a monomer in solution under the conditions where the structure was determined (2 mM, pH 5.1 at 30°C). Based on the structure and the amino acid sequence compared to other chemokines we propose that Ile20 and Leu25 in MCP-3 play key roles in the formation of N-loop (residues between the 2nd cysteine and the 1 sheet) which has been implicated as a determinant of chemokine specificity. Additional receptor binding surface is supplied by the 40s loop (residues between the 2 and the 3 sheet) and the binding interface of the acidic N-terminal region of chemokine receptor to MCP-3 would resemble the dimerization interface of CC type dimer.

Keywords : MCP(monocyte chemoattractant protein), IL-8 (interleukin-8), NMR HIV(human immunodeficiency virus), Monocyte chemoattractant protein-3

INTRODUCTION

Chemokines play key roles in the inflammatory host defense by attracting inflammatory cells to the sites of inflammation to help fight infections. However, this protective action can cause a wide range of inflammatory side effects such as allergy and auto-immune diseases.[1,2] Since the discovery of IL-8, tens of chemokines have been found

* To whom correspondence should be addressed. E-mail : keysun@kist.re.kr

in many types of cells. However, the functions of chemokines are highly redundant. With the exception of eotaxin, which activates only eosinophils, chemokines activate many cell types and many chemokines often share a common receptor.[3] Among them, RANTES and MCP-3 have the broadest spectrum of receptors. MCP-3, which was at first purified from cytokine-stimulated osteosarcoma cells (MG-63),[4] is highly homologous to MCP-1. However, its function is quite different. MCP-3 attracts many cell types including monocytes, dendritic cells, lymphocytes, natural killer cells, basophils, eosinophils, and neutrophils.[5] MCP-3 can bind to chemokine receptors CCR1, CCR2, and CCR3 whereas MCP-1 binds only to CCR2.[5] Gong & Clark-Lewis[6] showed that the N-terminal region of MCP-1 is critical for activity, but removal of the N-terminal of MCP-3 or MCP-1 does not change the specificity of MCP-3 or MCP-1[7] indicating that the determinants of specificity between MCP-3 and MCP-1 reside in other regions than the N-terminal. In conjunction with other results, the N-loop residues between the 2nd cyteine and the β1 sheet have been suggested to be involved in receptor binding.[8,9]

We previously reported that MCP-3 exists as a monomer at the concentration of as high as 2mM, and that the structure of MCP-3 is similar to other chemokines with disordered N- and C-termini.[10] However, the functionally critical N-loop was not well defined because of the lack of assignments in the N-loop. Meunier *et al*[11] have also reported a low resolution NMR solution structure of MCP-3 and argued that MCP-3 forms a IL-8 type dimer in contrast to our observations. Herein we report the high resolution solution structure of MCP-3 obtained from multinuclear, multidimensional NMR experiments using recombinant ^{13}C-, ^{15}N-doubly labeled protein. Based upon this structure we suggest the possible determinants of receptor binding specificity of MCP-3. With the recent surge of research regarding to the role of chemkines in inhibiting HIV infections,[12,13] the high resolution structure of MCP-3 could give valuable information in understanding the mechanism of chemokine-mediated signal transduction and the HIV infection.

MATERIALS AND METHODS

Sample Preparation

Recombinant human MCP-3 protein was prepared from MCP-3 gene (gift from Dr. Opdenakker) subcloned into an expression vector pET15b (Novagen) in *E. Coli* strain BL21 (DE3). When cell growth reached at the logarithmic phase at 37 °C, protein expression was induced by adding 0.4 mM IPTG for 3 hours. After harvesting cells, seven grams of harvested cell paste was suspended in 150 ml lysis buffer (100 mM Na-phosphate, pH8.0, 100 mM NaCl), frozen and then thawed in cold water. Tween X-100 (0.1%), Phenylmethyllsufonyl fluoride (0.5 mM), and glycerol (1%) were added to the thawed cell suspension and the cell extract was prepared by ultra-sonication. The extract was incubated on ice for 30 min with addition of 0.1% of $MgCl_2$ and 0.4% of Tween X-100, and centrifuged at 15,000 rpm for 30 min. The soluble fraction was applied to a 3 ml of Ni-NTA-agarose column (Qiagen) equilibrated with the lysis buffer. After the extensive washing of column, bound protein was eluted, cleaved with thrombin to remove histidine tag, and further purified by HPLC with C_{18} reverse phase column. Purified protein was lyophilized and stored at -20 °C. The uniform labeling of ^{13}C, ^{15}N of protein was achieved by growing cell in M9 minimal medium with 1g of $^{15}NH_4Cl$ and 2.0g of ^{15}C-glucose/ L.

NMR sample was prepared by dissolving about 10 mg of protein in 0.5 ml of either 90% H_2O/10% ^2H_2O or 99.9% ^2H_2O and pH was adjusted to 5.10 ± 0.05 (glass electrode, uncorrected) with concentrated NaO^2H.

NMR spectroscopy

The heteronuclear NMR experiments were carried out with an ^{15}N labeled sample or ^{13}C,^{15}N labeled sample in 90% H_2O / 10% ^2H_2O. All experiments were done using Varian UnityPlus 600 or Inova 500 spectrometers at a temperature of 30 °C. The concentration of protein was about 2 mM. Deuterium exchange of amide protons in MCP-3 was initiated by dissolving lyophilized sample in ^2H_2O, and 2D ^1H -^{15}N HSQC spectra was recorded at 20 °C. pH 5.1. 2D ^1H-^{13}C CT-HSQC, 3D ^1H -^{15}N NOESY-HSQC, ^1H -^{15}N TOCSY-HSQC,[14] HNHA [15] were acquired with the ^{13}C- or ^{15}N-labeled sample and ^{13}C- , ^{15}N-edited NOESY[16] and CBCA(CO)NH[17] were acquired with the ^{13}C, ^{15}N labeled sample. Heteronuclear NOE was measured with and without saturation of 3 sec.[18] NMR data were processed using a program NMRPipe.[19]

NOE Assignments and Distance Restraints

NOE distance restraints were derived from 3D ^{1}H-^{15}N NOESY-HSQC, ^{13}C-,^{15}N-edited NOESY, and ^{1}H NOESY spectra in $^{2}H_2O$ all with a mixing time of 150 ms. All NOE cross peaks were assigned using a program PIPP (provided by Dr. Dan Garrett). Ambiguous assignments were clarified gradually throughout structure calculations by use of a program STAPP included in PIPP package. The NOE intensity was converted into three groups of classes (1.8-2.7, 1.8-3.5, 1.8-5.0) and pseudo-atom corrections were made appropriately.[20]

Other Restraints

The scalar coupling constant of the α-proton to the amide proton was obtained from the HNHA experiments. The backbone torsion angle ϕ was restrained to -90 to -20 for $^{3}J_{HNH\alpha}$ <5.5Hz, -60 to -180 for $^{3}J_{HNH\alpha}$ 7-8Hz, -70 to -170 for $^{3}J_{HNH\alpha}$ 8-9 Hz, and -90 to -150 for $^{3}J_{HNH\alpha}$ >9Hz. Additionally if the intraresidue NOE between α-proton and amide proton was less intense than the interresidue NOE to preceding residue, ϕ torsion angle was restrained to -60 to -180.[21] The ψ torsion angles were restrained based on the ^{13}C chemical shifts of Cα and Cβ.[22] The side chain torsion angles χ_1 were restrained based on cross peak intensities deduced from ^{1}H-^{15}N HSQC-TOCSY, and ^{13}C-, ^{15}N-edited NOESY spectra. Additional backbone H-bond restraints were given where secondary structures were indicated based on NOE connectivity. For each hydrogen bond, two restraints (r_{NH-O}, 1.7-2.3; r_{N-O}, 2.5-3.3) were used. Additionally J-coupling constants,[23] carbon chemical shifts of Cα and Cβ resonances[24] and a database potential[25, 26] were directly included in the simulated annealing protocol.

RESULTS

Protein Purification

The expression of MCP-3 in *E. Coli* strain BL21(DE3) was good in the pET15b expression vector, but more than half of MCP-3 protein went into the insoluble fraction when the cell paste was lysed in normal buffer. Protein purified from the insoluble fraction by Ni-NTA-agarose column under denaturing conditions without DTT showed weak native

like resonances in NMR spectrum and was highly aggregative at pH 5.0. Refolding of this protein was successful with only low efficiency. However, MCP-3 purified from the soluble fraction showed native NMR resonances with expected intensities. Therefore we decided to increase the solubility of MCP-3 by changing pH and ionic strength of the cell lysis buffer. Consequently, 100 mM sodium phosphate with 100 mM NaCl at pH 8.0 was used as the lysis buffer. Specially the effect of ionic strength of lysis buffer was critical when M9 minimal medium is used for the culture. Purification of MCP-3 to higher than 95% was achieved by Ni-NTA-agarose column, thrombin digestion of the fused histidine tag, and C_{18} reverse phase HPLC. The final yield of MCP-3 was about 7mg/L. The expressed MCP-3 has a 4 residue Gly-Ser-His-Met N-terminal extension because of a cloning artifact.

NMR Assignments and Measurement of NOEs

Since the proton NMR chemical shifts of the recombinant MCP-3 were not different from the chemically synthesized MCP-3,[10] assignments of the ^{13}C and ^{15}N NMR chemical shifts were straightforward. All the assignments of ^{1}H, ^{13}C, and ^{15}N NMR chemicals shifts for MCP-3 at 30 °C and pH 5.1 were obtained by use of 3D ^{1}H-^{13}C, ^{1}H-^{15}N, and ^{1}H-^{13}C-^{15}N experiments. The amide proton of Tyr13 was in fast exchange with solvent and no correlation to it could be observed with presaturation experiments. However, it could be assigned from NOE peaks observed in pulsed field gradient experiments. Assignments of residues 19-22 which were uncertain in earlier ^{1}H NMR spectra[10] were confirmed by using CBCA(CO)NH experiments. The chemical shifts of protons of Lys19 (Hα = 2.52 ; Hβ~1ppm), Ile20 (HN = 6.4ppm), Lys22 (Hα = 3.24ppm) and Val60 (HN = 5.71ppm, Hγ = -0.67,0.42ppm) are highly up-field shifted as in other CC type chemokines[27] indicating the proximity of the aromatic rings of Trp59, Phe43 and Phe63.

The NOE connectivities shown in Fig. 1 indicate the existence of a helical turn between residues 22-25 and α-helix between residues 58-68. The 3 strand anti-parallel β-sheet is defined based on the NOE connectivities reported previously.[10] Additionally, a γ-turn is found between residues 54-56. Chemical shift index[28] and J-coupling constants are consistent with the secondary structures assigned. In deuterium exchange experiments, no amide protons were observed after 24 hrs at 30 °C, pH 5.1. However, the amide protons of residues in the hydrophobic core were observable after 40 min at 20 °C. The cross peaks

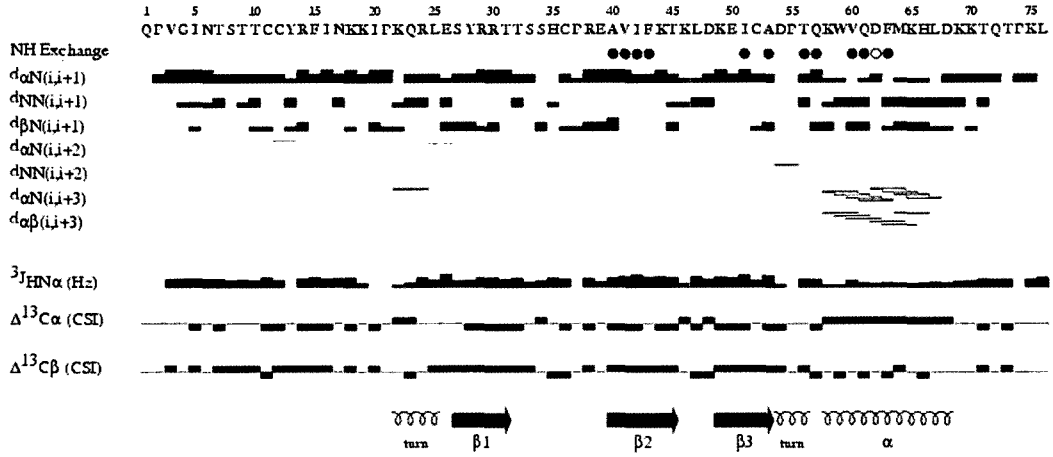

Fig. 1. Summary of short- and medium-range NOE, $^{3}J_{HNH\alpha}$ coupling constants, chemical shift index of $^{13}C\alpha$, $^{13}C\beta$,[28] and deuterium exchange. The cross peaks observed after 40 min at 20 °C, pH 5.1 in $^{2}H_2O$ are shown in circle. Weak peaks are in open circles. The thickness of line correlates with the intensity of NOE.

observed are Ala40, Val41, Ile42, Phe43, Ile51, Ala53, Thr56, Gln57, Val60, Gln61, Asp62, and Phe63. All these correspond to residues in strands β2, β3, and the helix with the exception of Thr56 and Gln57 that are in the γ-turn region. Fast exchange of amide protons are expected since the transition temperature of unfolding of MCP-3 measured by CD is around 49 °C under the conditions of NMR experiment. A total of 925 NOEs were assigned consisting of 149 long, 62 medium, 184 sequential, and 530 intra-residue NOEs. All restraints used in the structural calculations are summarized in Table 1.

Structure Calculations

Structure calculations of MCP-3 were carried out using a hybrid protocol of distance geometry and simulated annealing using the program XPLOR.[29] When an initial structure was obtained, J-coupling constants, Cα and Cβ chemical shifts, and a database potential was included to calculate the final structure. When calculations were done without a database potential, the geometric quality that estimated by the program PROCHECK[30] was not very good. However, when the database potential [30,26] was included in the simulated annealing

Table 1. Summary of structural restraints derived from NOEs, coupling constants, and chemical shifts.

Distance restraints:	
Intra-residual	530
Sequential	184
Medium-range ($1 < \|i-j\| < 5$)	62
Long-range ($\|i-j\| > 4$)	149
Hydrogen bonds	2*16
Angular restraints:	
Dihedral angle ϕ	66
Dihedral angle ψ	33
Dihedral angle χ_1	36
Coupling constants	68
Chemical shifts	74

For each hydrogen bond, two distance restraints are used : r_{HN-O} 1.7-2.3, r_{N-O} 2.5-3.3. Coupling constants and chemical shifts are used for restraints based on references 23,24. Chemical shifts restraints are ^{13}C chemical shifts of C_α and C_β of each residue refenced from DSS at 30 °C. Coupling constants are values obtained from HNHA experiments.

Table 2. Summary of the statistics for the 20 final structures.

Atomic rmsd values (Å)	
Backbone atoms	0.55
All heavy atoms	1.14
X-PLOR energy terms (kcal/mol)	
E_{tot}	-276 ± 51
E_{bond}	17 ± 1
E_{angl}	147 ± 6
E_{impr}	21 ± 1
E_{vdw}	-505 ± 50
E_{cdih}	0.5 ± 0.3
E_{NOE}	44 ± 4

The values for rmsd are from the residues 11-68. The values for X-PLOR energy terms were obtained with force constants of 4 kcal/mol/Å^4 (E_{vdw}), 50 kcal/mol/Å^2 (E_{NOE}), and 200 kcal/mol (E_{cdih}). E_{vdw} energy is L-J energy of X-PLOR energy terms.

protocol, the geometric quality improved significantly. Specially the improvement of side chain geometry was remarkable (4Å rmsd to 1Å rmsd). The rmsd atomic displacements of residues 11-68 are 0.55 Å for backbone atoms and 1.14 Å for all heavy atoms. More than 85% of ϕ, ψ angles of all 20 structures are in the most favored region in the Ramachanran plot and no disallowed ϕ, ψ angles are found. The statistics of the ensemble of 20 structures are shown in Table 2.

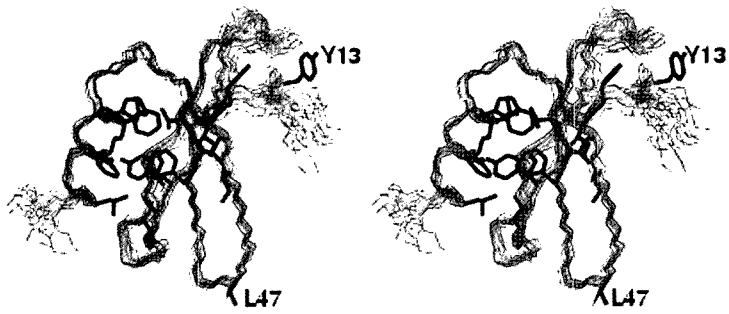

(a)

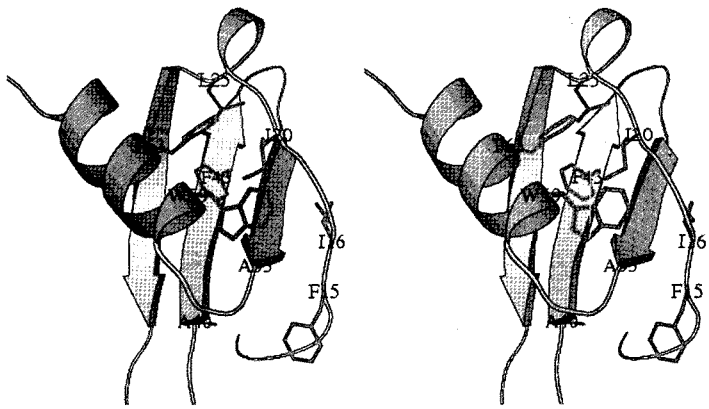

(b)

Fig. 2. Stereoviews and MOLSCRIPT (42) representations of MCP-3 with hydrophobic side chains. (a) An ensemble of 20 structures of MCP-3 with hydrophobic side chains. The exposed hydrophobic residues (more than 50 % of side chain) are labeled. (b) Interactions of the N-loop with the rest of the structure. Hydrophobic residues involved in interactions of the N-loop is labeled. Disulfide bridges are in gold.

Solution Structure

The solution structure of MCP-3 consists of 3 strands of β-sheet and a C-terminal helix similar to that reported for other chemokines. However, when compared to other CC chemokines, N-terminal residues are disordered. As shown in Fig. 2a, the many of the residues in the structured region are involved in hydrophobic interactions. However, Tyr13

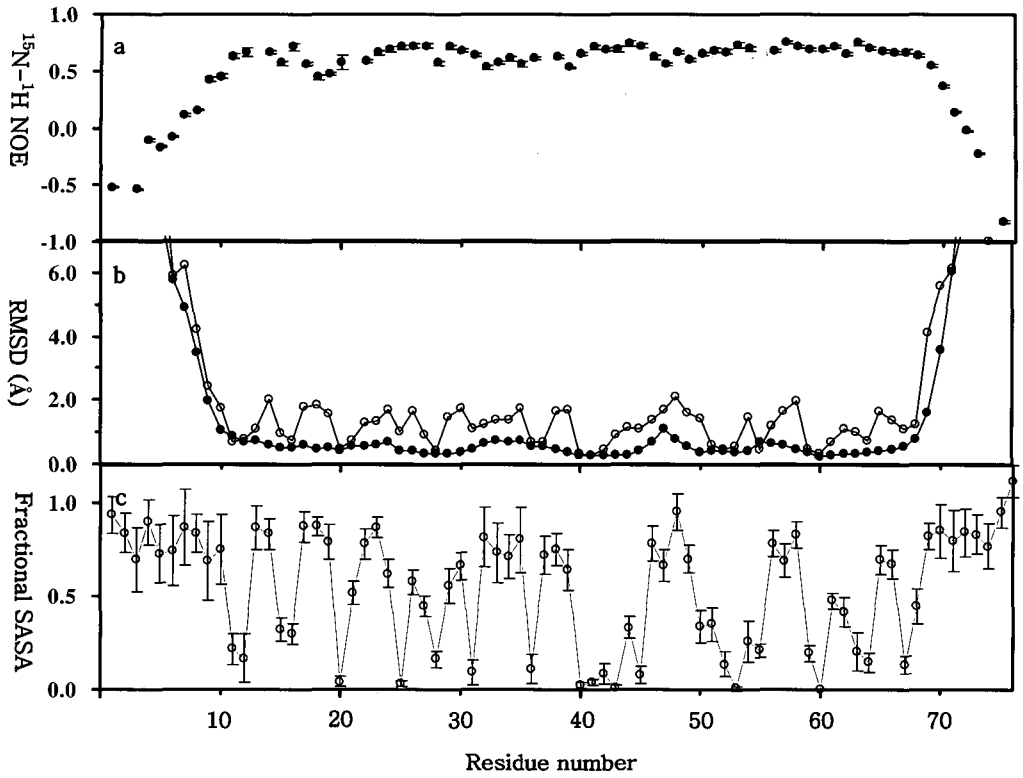

Fig. 3. The atomic displacements of the backbone and side chain atoms and dynamics of backbone. a) The ratio of ^{15}N-^{1}H heteronuclear NOE. The ratio of ^{15}N-^{1}H heteronuclear NOE intensity with and without saturation was shown. b) The rmsd atomic displacements of backbone (●) and side chain (O) atoms from the mean of the ensemble. c) Average fractional solvent accessible area of side chains of 20 structures. Standard deviations are shown with bar.

and Leu47 are exposed to the solvent implying possible roles other than protein stability. The N-loop (residues between the 2nd cysteine and the β1 sheet) is well defined compared to our previous structure[10] by the interactions of Phe15, Ile16, Ile20, and Leu25 with other hydrophobic residues in the β2, β3, and C-terminal helix as shown in Fig. 2b. Strands β1, β2, and β3 act as a base to the N-loop and the C-terminal helix. The N-loop and the C-terminal helix are anchored to the strands by hydrophobic interactions. Residues Ile20 and Leu25 form the hydrophobic core with other hydrophobic residues in the beta sheet and

helix. The rmsd atomic displacements for the 20 low energy structures (Fig. 3b) indicates that the secondary structure elements are well defined, but the loop regions are less well defined. The solvent accessible surface areas (Fig. 3c) indicate that all hydrophobic residues are well buried other than Tyr13 and Leu47. The backbone dynamics investigated by ^{15}N-^{1}H heteronuclear NOE measurements (Fig. 3a) indicate that the protein is rigid on the picosecond-nanosecond time scale with the exception of the N- and C-termini which are quite flexible. The N-, 30s (residues between the β1 and β2 sheet), and 40s (residues between the β2 and β3 sheet) loops are relatively flexible compared to the secondary structured regions. Deuterium exchange indicates that strand β1 and the end of α-helix are more dynamic on the slower time scales (Fig. 1).

DISCUSSION

MCP-3 is a monomer

The quaternary structures of known structures are diverse depending on the intrinsic properties of chemokines and the conditions under which structures were solved. The CXC family chemokines such as IL-8 and GRO-α form dimers under conditions where structures were determined.[31-34] The dimeric interactions of these chemokines exist between the β-sheets resulting in 6 anti-parallel sheet. On the other hand, the CC chemokines such as MIP-1β,[35] RANTES,[36, 37] and MCP-1[27] form dimers by interactions between the N-terminal regions resulting in a head-to-head dimer. Further more, the crystal structure of MCP-1 has been shown to exist as both monomer and dimer [38] and that of NAP-2 was shown to be a tetramer.[39] The inter-subunit interactions of CC type dimer such as MCP-1, MIP-1β are the hydrophobic interactions between the N-loop (residues between the 2nd cysteine and the β1 sheet) and the N-terminal (residues before the 1st cysteine) or the 30s loop (residues between β1 and β2 sheet). But in RANTES, electrostatic interactions between the N-terminal and starnd β3 contribute to the dimer formation. In CC type chemokines, the residues involved in dimer interactions are diverse resulting in the quite different quarternary structures even though they retain a head-to-head dimer scaffold. The long range interactions of the CXC type dimer that result in 6 anti-parallel β-sheet can be attributed to the interaction between

hydrophobic residues in the C-terminal helix and β1 strand. In most CXC type chemokines, these interactions are retained resulting in the very similar quarternary structures. In the case of IL-8, the interactions between Phe65 and Leu66 in the C-terminal helix and Val27 in the β1 strand of the other subunit contribute to dimer formation. The dimer of IL-8 is further stabilized by the electrostatic interactions between Glu24 and Arg26. In the case of NAP-2 and bPF-4, both CC and CXC type of interactions are found. In the case of SDF-1, residue types at the corresponding positions are consistent with the dimer formation but the interaction angle between β-sheet and the C-terminal helix is known to be different[40] probably because of the bulky hydrophobic Leu55 resulting in a monomer. In Fig. 4, the residues involved in long range quarternary interactions of the chemokines of known structures are shown. Interactions indicated in Fig. 4 might not be all the long-range interactions that take part in oligomerization but MCP-3 does not have any similar type of residues at the corresponding positions. We think that MCP-3 is a monomer because it does not have the proper residues at the corresponding positions to induce dimer interactions. The side chain of Tyr13 is exposed to the bulk water in MCP-3 compared to other CC chemokines where it interacts with N-terminal hydrophobic residues playing a role in dimer formation. Backbone dynamics measured by heteronuclear NOE (Fig. 3a) also indicates that the N-terminal is disordered showing very low or negative NOE ratio in contrast to other CC type chemokines. The short C-terminal helix also excludes the possibility of CXC type dimer formation. The size of MCP-3 was determined by the relaxation measurement where the ^{1}H-^{15}N heteronuclear T_1/T_2 ratio is 4.34±0.78 corresponding to the rotation correlation time of 5.72±0.71 nsec. The rotation correlation time of 5.72 nsec corresponds to the radius of gyration 17.9Å which is close to actual radius of monomeric MCP-3 considering hydration shell. Recently Meunier et al. [11] reported that MCP-3 forms the CXC type dimer. The aggregation profile mentioned by the authors is very similar to that of the protein we obtained from inclusion bodies, which tends to aggregate at pH 5.1 and has very low intensity native NMR peaks. The protein we used for structure calculations has transition temperature of 49 °C with two state behaviors indicating a properly folded protein (data not shown).

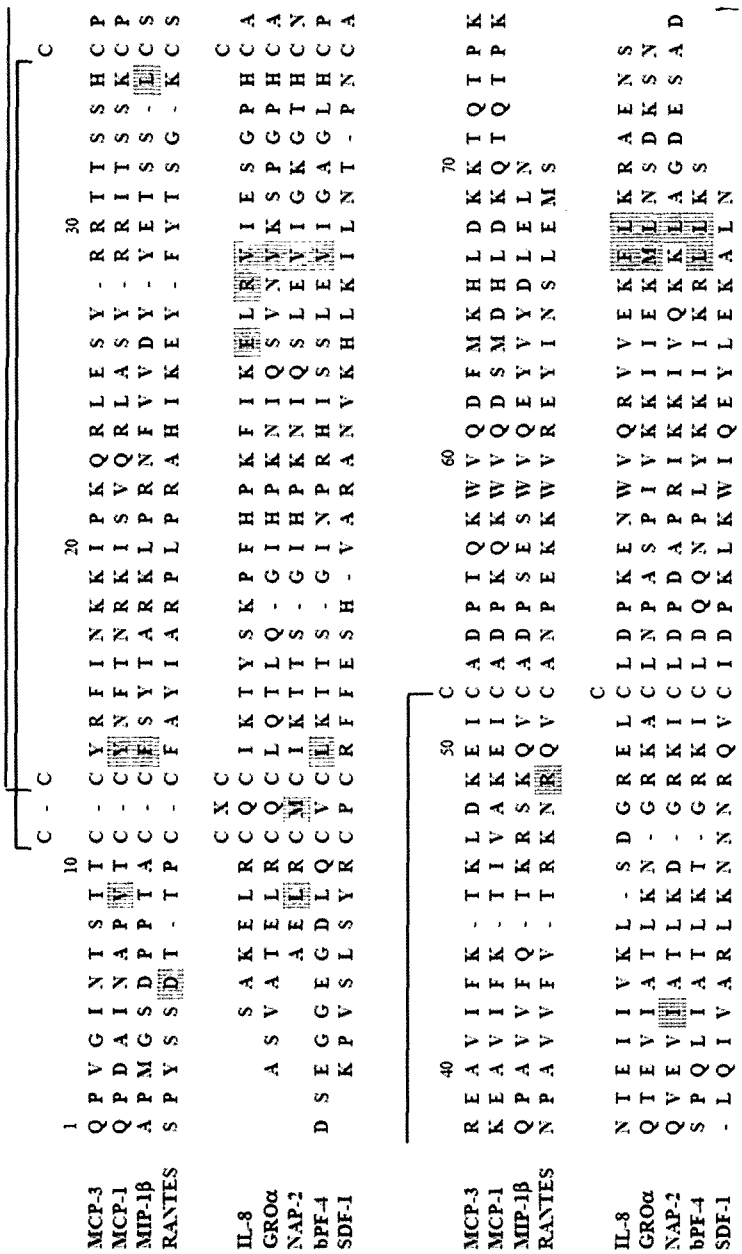

Fig. 4. Sequence alignments of chemokines of known 3-dimensional structures. The residues involved in the inter-subunit hydrophobic or electrostatic interactions are shaded.

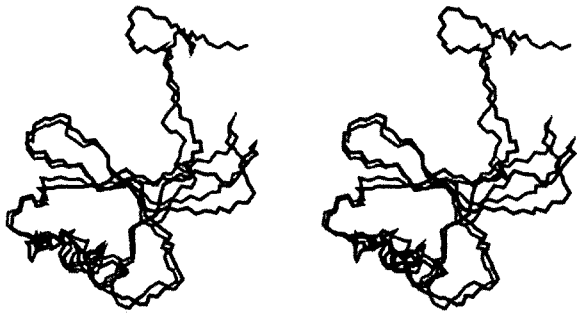

Fig. 5. Superposition of MCP-3 and RANTES. Backbone atoms of N, C_α, C of residues 12-32 and 40-68 of MCP-3 (solid) are superposed on the corresponding residues (residues 11-31, 38-66) of RANTES (gray). The rmsd between MCP-3 and RANTES is 1.4 Å.

N-terminal and N-loop in MCP-3

MCP-1 and MCP-3 share the receptor CCR-2, MCP-3 and RANTES share the receptors CCR-1 and CCR-3, and MIP-1β and RANTES share the receptor CCR-5. Overall, the structures of these chemokines are very similar. When the Cα atoms of MCP-3 (residues between 12 to 32, and 40 to 68 of the monomer) were compared to the corresponding regions of the other chemokines, the rmsd to MCP-1, MIP-1β, and RANTES are 1.5, 1.7, and 1.4 Å, respectively, and do not correlate to the receptor binding pattern. The differences in the N-terminal and 30s loop (residues between strands β1 and β2 of the β sheet) are pronounced. However, the differences in the N-terminal and 30s loop may arise from the differences in subunit interactions. Considering that MCP-3 exists as a monomer and the other chemokines are known to exist as dimers under the conditions where structures were determined, the differences in N-terminal backbone structures are unlikely to be related to the function of these chemokines. In Fig. 5, the superposition of MCP-3 and RANTES shows the typical pattern of structural difference observed among chemokines.

On the other hand, specific interactions of side chains of residues in the chemokine with the respective chemokine receptors are expected to be key determinants of receptor specificity considering that most chemokines have highly similar global structure. The N-

loop of MCP-3 is well defined and its structure is similar to other chemokine structures. The N-loop is confined by the 2nd cysteine and strand β1 of the β sheet. The interactions involved in structure formation of the N-loop are hydrophobic interactions involving Ile20 and Leu25 These two residues are conserved in all chemokines known thus far. The extensive interactions of these two residues with hydrophobic residues in the β-sheet and the C-terminal helix are observed in all known chemokine structures. These interactions create part of a hydrophobic core and are manifested by the unusual chemical shifts of several amino acids in the loop (Lys19, Ile20, and Lys22) and the C-terminal helix (Val60) due to the 'ring current effect' of Phe43, Trp59, and Phe63. Additionally Ile16 interacts with Ile51. Mutations of Ile15 and Leu19 [9] in RANTES, which correspond to Ile16 and Leu20 in MCP-3, showed that binding affinity for CCR-5 was significantly affected, whereas affinity for CCR-3 was affected noticeably only in the case of Ile15 mutation, and affinity for CCR-1 was hardly affected with either mutations. Other residues affecting on binding affinity in the N-loop of RANTES [9] are mostly exposed in MCP-3 as well as in a monomer structure of RANTES. In MCP-3, the basic contiguous surface shown in Fig. 6 is formed by the N-loop and 40s loop (residues between β2 and β3 sheet). Considering that the acidic N-terminal region of the chemokine receptors is involved in binding, this contiguous basic surface in MCP-3 is likely to be involved in receptor binding. In addition to the positively charged residues, highly exposed hydrophobic residues, Tyr13 and Leu47, reside in these regions. The highly exposed hydrophobic residue, Phe12 in RANTES, has been shown to be critical in receptor binding.[9] Therefore we propose that 40s loop as well as the N-terminal and the N-loop be involved in receptor binding in MCP-3. Considered this binding surface, the binding pattern between MCP-3 and the N-terminal of MCP-3 receptor is expected to be similar to dimerization interface of the CC type chemokines. These proposed binding sites of the N-terminal region of receptor are consistent with the regions that have the chemical shift perturbation in IL-8 when the N-terminal peptide of IL-8 receptor was bound.[41]

In conclusion, MCP-3 uses its plastic regions such as the N-terminal, the N-loop, and 40s loop for various receptor binding. And the plasticity of chemokine could be a key factor for adjustability of multivalent chemokines such as MCP-3, RANTES, and vMIPII.

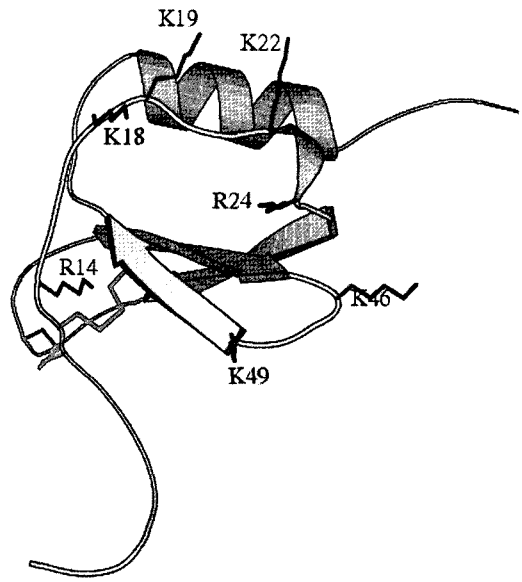

(a)

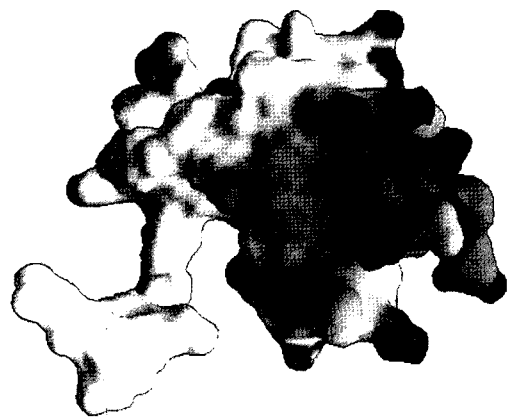

(b)

Fig. 6. The positively charged surface suggested to be involved in receptor binding. (a) The positively charged residues in the N-loop and the 40s loop, and Lys49 are labeled. Tyr13 and Leu47 are not shown but are in the same surface. (b) Potential surface of MCP-3 in similar orientation generated by a program GRASP (43). Positive potential is in blue and negative potential is in red.

Acknowledgements

The authors thank Dr. K.B. Lee and S. Gagné for the help with NMR experiments and Drs M. Crump and K. Rajarathnam for helpful discussion. We acknowledge Dr. G.M. Clore for allowing us to access his database potential library; Dr. L. E. Kay for pulse sequences; Dr. D. Garrett for the program PIPP; and Dr. Opdenakker for the gift of the MCP-3 gene.

Abbreviations:

MCP, monocyte chemoattractant protein; IL-8, interleukin-8; RANTES, regulated upon activation, normal T-cell expressed and presumably secreted; MIP, macrophage inflammatory protein; HIV, human immunodeficiency virus; NAP, neutrophil-activating peptide; bPF, bovine platelet factor; SDF, stromal cell-derived factor; IPTG, isopropyl β-D-thiogalactopyranoside; NMR, nuclear magnetic resonance; NOE, nuclear Overhaser effect; NOESY, nuclear Overhauser enhancement spectroscopy; HSQC, heteronuclear single-quamtum coherence; TOCSY, total correlation spectorscopy; DTT, dithiothreitol; HPLC, high performace liquid chromatography; rmsd, root mean square difference; CD, circulat dichroism

REFERENCES

1. Baggiolini, M., Dewald, B., and Moser, B. *Adv. Immunol.* **55,** 97-179 (1994).
2. Miller, M. D., and Krangel, M. S. *Crit. Rev. Immunol.* **12,** 17-46 (1992).
3. Premack, B. A., and Schall, T. J. *Nature Medicine* **2,** 1174-1178 (1996).
4. Van Damme, J., Proost, P., Lenaerts, J. P., and Opdenakker, G. J. *Exp Med* **176,** 59-65 (1992).
5. Proost, P., Wuyts, A., and Van Damme, J. *J Leukoc Biol* **59,** 67-74 (1996).
6. Gong, J. H., and Clark-Lewis, I. *J Exp Med* **181,** 631-40 (1995).
7. Gong, J. H., Uguccioni, M., Dewald, B., Baggiolini, M., and Clark-Lewis, I. *J Biol Chem* **271,** 10521-10527 (1996).
8. Clark-Lewis, I., Kim, K.-S., Rajarathnam, K., Gong, J.-H., Dewald, B., Moser, B.,

Baggiolini, M., and Sykes, B. D. *J. Leukoc. Biol.* **57,** 703-711 (1995).

9. Pakianathnan, D. R., Kuta, E. G., Artis, D. R., Skelton, N. J., and Hébert, C. A. *Biochemistry* **36,** 9642-9648 (1997).
10. Kim, K.-S., Rajarathnam, K., Clark-Lewis, I., and Sykes, B. D. *FEBS Lett* **395,** 277-282 (1996).
11. Meunier, S., Bernassau, J. M., Guillemot, J. C., Ferrara, P., and Darbon, H. *Biochemistry* **36,** 4412-22 (1997).
12. Bleul, C. C., Farzan, M., Choe, H., Parolin, C., Clark-Lewis, I., Sodroski, J., and Springer, T. A. *Nature* **382,** 829-836 (1996).
13. Cocchi, F., DeVico, A. L., Garzino-Demo, A., Arya, S. K., Gallo, R. C., and Lusso, P. *Science* **270,** 1811-1815 (1995).
14. Zang, O., Kay, L. E., Oliver, J. P., and Forman-Kay, J. D. *J. Biomol. NMR* **4,** 845-858 (1994).
15. Kuboniwa, H., Grzesiek, S., Delaglio, F., and Bax, A. *J. Biomol. NMR* **4,** 871-878 (1994).
16. Pascal, S. M., Muhandiram, D. R., Yamazaki, T., Forman-Kay, J. D., and Kay, L. E. *J. Magn. Reson. Series B* **103,** 197-201 (1994).
17. Muhandiram, D. R., and Kay, L. E. *J. Magn. Reson. Series B.* **103,** 203-216 (1994).
18. Farrow, N. A., Muhandiram, R, Singer, A. U., Pascal, S. M., Kay, C. M., Gish, G., Shoelson, S. E., Pawson, T., Forman-Kay, J. D., and Kay, L. E. *Biochemistry* **33,** 5984-6003 (1994).
19. Delaglio, F., Grzesiek, S., Vuister, G. W., Zhu, G., Pfeifer, J., and Bax, A. *J. Biomol. NMR* **6,** 277-293 (1995).
20. Wüthrich, K., Billeter, M., and Braun, W. *J. Mol. Biol.* **169,** 949-961 (1983).
21. Clubb, R. T., Ferguson, S. B., Walsh, C. T., and Wagner, G. *Biochemistry* **33,** 2761-2722 (1994).
22. Spera, S., and Bax, A. *J. Am. Chem. Soc.* **113,** 5490-5492 (1991).
23. Garrett, D. S., Kuszewski, J., Hancock, T. J., Lodi, P. J., Vuister, G. W., Gronenborn, A. M., and Clore, G. M. *J. Magn. Reson. Series B* **103,** 99-103 (1994).
24. Kszewski, J., Qin, J., Gronenborn, A. M., and Clore, G. M. *J. Magn. Reson. Series B* **106,** 92-96 (1995).

25. Kszewski, J., Gronenborn, A.M., and Clore, G. M. *J. Magn. Reson.* **125,** 171-177 (1997).
26. Kszewski, J., Qin, J., Gronenborn, A. M., and Clore, G. M. *Protein Sci.* **5,** 1067-1080 (1996).
27. Handel, T. M., and Domaille, P. J. *Biochemistry* **35**(21), 6569-6584 (1996).
28. Wishart, D. S., and Sykes, B. D. *Methods Enzymol.* **239,** 363-392 (1994).
29. Brünger, A. T. (1993) *X-PLOR manual Version 3.1,* Yale University, New Haven, CT.
30. Laskowski, R. A., Rullmannn, J. A., MacArthur, M. W., Kaptein, R., and Thornton, J. M. *J Biomol NMR* **8,** 477-486 (1996).
31. Clore, G. M., Appella, E., Yamada, M., Matsushima, K., and Gronenborn, A. M. *Biochemistry* **29,** 1689-1696 (1990).
32. Baldwin, E. T., Weber, I. T., Charles, R. S., Xuan, J.-C., Appella, E., Yamada, M., Matsushima, K., Edwards, B. F. P., Clore, G. M., Gronenborn, A. M., and Wlodawer, A. *Proc. Natl. Acad. Sci. USA* **88,** 502-506 (1991).
33. Fairbrother, W. J., Reilly, D, Colby, T., Hesselgesser, J., and Horuk, R. *J. Mol. Biol.* **242,** 252-270 (1994).
34. Kim, K.-S., Clark-Lewis, I., and Sykes, B. D. *J. Biol. Chem.* **269,** 32909-32915 (1994).
35. Lodi, P. J., Garret, D. S., Kuszewski, J., Tsang, M. L.-S., Weatherbee, J. A., Leonard, W. J., Gronenborn, A. M., and Clore, G. M. *Science* **263,** 1762-1767 (1994).
36. Skelton, N. J., Aspiras, F., Ogez, J., and Schall, T. J. *Biochemistry* **34**(16), 5329-5342 (1995).
37. Chung, C. W., Cooke, R. M., Proudfoot, A. E., and Wells, T. N. *Biochemistry* **34**(29), 9307-9314 (1995).
38. Lubkowski, J., Bujacz, G., Boque, L., Domaille, P. J., Handel, T. M., and Wlodawer, A. *Nat Struc. Biol.* **4,** 64-69 (1997).
39. Malokowski, M. G., Wu, J. Y., Jphnson, P. H., and Edward, B. F. *J. Biol. Chem.* **270,** 7077-7087 (1995).
40. Crump, M. P., Gong, J.-H., Loetscher, P., Rajarathnam, K., Amara, A., Arenzana-Seisdedos, F., Virelizier, J.-L., Baggiolini, M., Sykes, B. D., and Clark-Lewis, I. *EMBO* **16,** 6996-7007 (1997).

41. Clubb, R. T., Omichinski, J. G., Clore, G. M., and Gronenborn, A. M. *FEBS letters* **338,** 93-97 (1994).
42. Kraulis, P.J. *J. Appl. Crystallogr.* **24**, 946-950 (1991).
43. Nicholls, A., Sharp, K.A., and Honig, B. *Proteins* **11**, 281-296 (1991).